Inorganica Chimica Acta 479 (2018) 97–105

Contents lists available at ScienceDirect

Inorganica Chimica Acta

journal homepage: www.elsevier.com/locate/ica

Research paper

Utilisation of new NiSNS pincer complexes in paraffin oxidation

Lynette Soobramoney, Muhammad D. Bala *, Holger B. Friedrich *

School of Chemistry and Physics, University of KwaZulu-Natal, Private Bag X54001, Durban 4000, South Africa

ARTICLE INFO

Article history:
Received 17 October 2017
Received in revised form 12 April 2018
Accepted 18 April 2018
Available online 23 April 2018

Keywords:
Homogeneous catalysis
SNS ligand
Nickel catalyst
n-alkane
Oxidation

ABSTRACT

Two series of closely related SNS pincer ligands (L) were synthesised with the major structural variation on the nitrogen backbone containing either the methyl [L = $(RSCH_2CH_2)_2NMe$: where R = Me (**1**), Et (**2**), Bu (**3**)] or the phenyl [L = $(RSCH_2CH_2)_2NPh$: where R = Me (**4**), Et (**5**), Cy (**6**)] functional group. When ligands **1**–**3** were complexed to Ni by reaction with $Ni(DME)Cl_2$ (DME = dimethoxyethane), they respectively yielded three new cationic dimeric $[LNi(\mu\text{-}Cl)_3NiL]^+$ complexes (**7**–**9**), whilst ligands **4**–**6** on reaction with $Ni(PPh_3)_2Br_2$ respectively yielded neutral mononuclear ($LNiBr_2$) complexes **10**–**12**. All the new compounds were characterised by IR, HRMS, elemental analysis and in addition, single crystal X-ray diffraction for complexes **9**–**12**. X-ray structural data of **9** revealed an unusual three chlorido-bridged Ni dimer with the SNS ligand coordinated in a facial binding mode to the two pseudo-octahedral Ni centres. Molecular structures of complexes **10**, **11** and **12** each displayed five-coordinate distorted trigonal bipyramidal geometry around the nickel(II) metal centres. When utilised as catalysts in the tert-butyl hydroperoxide oxidation of *n*-octane, all the complexes showed activity to mainly products of internal carbon activation (octanones and secondary octanols) with **11** as the most active (10% total substrate to oxygenates yield), whereas **10** was the least active, but most selective towards alcohols (alcohol/ketone = 2.13).

1. Introduction

Exploration of the coordination chemistry and potential applications of pincer compounds has become a dynamic area of research over the last few decades [1–21]. In addition to the greater stability brought about by the (tridentate) binding mode of a pincer ligand, control over the electronic and steric properties of their metal complexes is one of the desirable features that made this type of ligands so popular [5,22–24]. More specifically, sulfur and nitrogen based pincer ligands are considered hemilabile due to dissimilarities in the donor strengths of the two coordinating atoms i.e. the relatively soft sulfur donor combined with a hard nitrogen donor. This feature is especially beneficial in catalysis as it offers a balance between high reactivity and stability of the metal complex [25]. Complexes bearing the SNS pincer moiety have found applications in catalytic reactions such as ethylene trimerization, [26–32] Suzuki coupling, [33] and transfer hydrogenation, [34] as well as in medicinal applications where SNS pincer complexes of radioactive metals were used as brain imaging agents [35–38].

In a previous work [39] we reported new CoSNS complexes with two types of known SNS ligands; [30,40–43] the first series were characterised by a rigid backbone (with a central pyridine moiety as the *N*-donor atom), while the second series contained a more flexible backbone symmetrically built around an amine *N*-donor atom. In both series, simple alkyl groups (respectively methylene and ethylene) served as linkers to the S-donor atoms. When we tested the complexes as catalysts in the oxidation of *n*-octane, the results showed that those with the flexible backbone were more active as catalysts. This observation prompted us to further explore relatively flexible variants of the SNS ligands, i.e. those constructed around a central amine N donor atom. For the current studies, additional functionalities (alkyl and aryl groups) were introduced on the central *N*-donor atom to allow for further modulation of its binding potentials to metal centres. A search of the literature revealed a paucity of reports [44–46] on the types of SNS ligands synthesized and reported in this work, hence many of the compounds are reported for the first time. Herein, we describe the synthetic protocols and characterisation of six SNS ligands and their coordination to nickel to yield a total of six new complexes. A complete study on their structural properties and catalytic application in the oxidation of *n*-octane is also reported and discussed.

* Corresponding authors.
E-mail addresses: bala@ukzn.ac.za (M.D. Bala), friedric@ukzn.ac.za (H.B. Friedrich).

https://doi.org/10.1016/j.ica.2018.04.033
0020-1693/

2. Experimental section

2.1. General

All reactions and manipulations were performed using standard Schlenk techniques under nitrogen atmosphere. Solvents were dried according to established methods, [47] and purged with high purity nitrogen gas prior to use. Diethyl ether (Et_2O) and tetrahydrofuran (THF) were dried over sodium wire and benzophenone, absolute ethanol (EtOH) and methanol (MeOH) were dried over magnesium turnings and iodine, while dichloromethane (DCM) was dried over phosphorous pentoxide. $Ni(DME)Cl_2$ was synthesized according to a procedure adapted from the literature, [48] whilst $Ni(PPh_3)_2Br_2$ was purchased from Sigma. All other reagents were obtained commercially and used as received. All NMR spectra were recorded using a Bruker Avance III 400 MHz spectrometer at ambient temperature. The ^1H NMR data are reported as chemical shift (δ, ppm) and referenced to the solvent peak $CDCl_3$. The attached proton test (APT) ^{13}C NMR, which distinguishes between quaternary C, CH, CH_2 and CH_3 carbons, are listed as chemical shift (δ, ppm) and positive (pos) or negative (neg) with the corresponding carbons in parentheses and referenced to the solvent peak $CDCl_3$. The IR data were recorded on a Perkin Elmer Attenuated Total Reflectance (ATR) spectrophotometer and elemental analyses were performed on a Thermo-Scientific Flash 2000 CHNS/O elemental analyzer, the HRMS was recorded on a Waters Micromass LCT Premier TOF-MS, while the melting points were determined using a Stuart Scientific melting point apparatus.

2.2. Bis(2-chloroethyl)methylamine

Into a 250 ml Schlenk flask containing 50 ml of DCM and 13.8 ml (120 mmol) of methyldiethanolamine, 26.0 ml (360 mmol) of $SOCl_2$ was added dropwise at 0 °C under vigorous stirring. The resultant solution was stirred at room temperature for 2 h, after which the solvent was removed *in vacuo* to yield a white solid which was dried under vacuum for several days. Yield: 98%. ^1H NMR (400 MHz, CD_3OD): δ 3.04 (s, 3H, C*H*$_3$-N), 3.69 (t, 4H, CH_2CH_2-N), 4.03 (t, 4H, CH_2CH_2-N). ^{13}C APT NMR (400 MHz, CD_3OD): δ 38.14 (CH_2CH_2-N) pos, 41.44 (CH_3-N) neg, 58.22 (CH_2CH_2-N) pos. Melting point = 106–107 °C.

2.3. Bis(2-tosylethyl)phenylamine (Ph-Tos)

In a 500 ml round bottom flask, phenyldiethanolamine (10.54 g, 58.2 mmol) was dissolved in 100 ml of THF. In a separate beaker, 23.92 g (598 mmol) of NaOH was dissolved in 100 ml of double-distilled water and added to the THF solution. A solution of tosyl chloride (22.02 g, 116 mmol) in 100 ml of THF was added slowly to the resultant mixture at 0 °C, which was then allowed to stir at 0 °C for 30 min and thereafter at room temperature for a total time of 4 h. The mixture was then poured into 200 ml of double-distilled water and extracted with DCM (3 × 100 ml). The combined organic fractions were then washed with a saturated NaCl solution, dried with $MgSO_4$ and evacuated to yield a peach colored oil which, upon standing overnight, turned into a solid. After recrystallization from DCM and EtOH, a white crystalline product was obtained. Yield: 71%. ^1H NMR (400 MHz, $CDCl_3$): δ 2.44 (s, 6H, C*H*$_3$-tosyl), 3.56 (t, 4H, CH_2CH_2-N), 4.10 (t, 4H, CH_2CH_2-N), 6.44 (d, 2H, aromatic), 6.72 (t, 1H, aromatic), 7.14 (t, 2H, aromatic), 7.28 (d, 4H, aromatic), 7.72 (d, 4H, aromatic). ^{13}C APT NMR (400 MHz, $CDCl_3$): δ 21.65 (CH_3-tosyl) neg, 50.19 (CH_2CH_2-N) pos, 66.58 (CH_2CH_2-N) pos, 112.03 (aromatic) neg, 117.61 (aromatic) neg, 127.84 (aromatic) neg, 129.48 (aromatic) neg, 129.89 (aromatic) neg, 132.62 (aromatic) pos. Melting point = 88–89 °C.

2.4. Bis(methylthioethyl)methylamine (1)

Sodium methanethiolate (3.38 g, 48.2 mmol) was added to a solution of bis(2-chloroethyl)methylamine (2.64 g, 16.9 mmol) in EtOH (50 ml) and the resultant mixture was refluxed for 2 h. The solvent was removed *in vacuo* and the cream residue was purified by elution with 5% MeOH in DCM through a silica column to yield a pale yellow oil. Yield: 71%. ^1H NMR (400 MHz, $CDCl_3$): δ 2.10 (s, 6H, C*H*$_3$-S), 2.27 (s, 3H, C*H*$_3$-N), 2.62–2.56 (m, 8H, CH_2CH_2-N). ^{13}C APT NMR (400 MHz, $CDCl_3$): δ 15.83 (CH_3-S) neg, 31.78 (CH_2CH_2-N) pos, 42.03 (CH_3-N) neg, 56.95 (CH_2CH_2-N) pos. HRMS ESI (*m*/*z*) Calcd for: $C_7H_{18}NS_2$ = 180.0881. Found: 180.0879. IR ν_{max} (cm^{-1}): 2956 (m), 2915 (s), 2843 (m), 2788 (m), 1456 (m), 1437 (m), 1110 (s), 699 (m).

2.5. Bis(ethylthioethyl)methylamine (2)

Sodium metal (1.101 g, 47.9 mmol) and ethanethiol (3.6 ml, 47.9 mmol) were stirred together in EtOH (50 ml) under inert atmosphere for 15 min in a 100 ml Schlenk flask. This mixture was then transferred to a solution of bis(2-chloroethyl)methylamine (2.49 g, 15.9 mmol) in EtOH (100 ml) via cannula and the resultant solution was refluxed for 2 h whilst monitoring by TLC. The solvent was then evacuated and the cream residue was purified analogously to **1** to obtain a pale yellow oil. Yield: 73%. ^1H NMR (400 MHz, $CDCl_3$): δ 1.24 (t, 6H, CH_3CH_2-S, *J* = 7.4 Hz), 2.28 (s, 3H, C*H*$_3$-N), 2.53 (q, 4H, CH_3CH_2-S), 2.63–2.59 (m, 8H, CH_2CH_2-N). ^{13}C APT NMR (400 MHz, $CDCl_3$): δ 14.87 (CH_3CH_2-S) neg, 26.21 (CH_3CH_2-S) pos, 29.22 (CH_2CH_2-N) pos, 42.05 (CH_3-N) neg, 57.41 (CH_2CH_2-N) pos. HRMS ESI (*m*/*z*) Calcd for: $C_9H_{22}NS_2$ = 208.1194. Found: 209.1190. IR ν_{max} (cm^{-1}): 2961 (m), 2925 (s), 2871 (w), 2846 (w), 2790 (m), 1453 (s), 1109 (m), 733 (m).

2.6. Bis(butylthioethyl)methylamine (3)

This ligand was synthesized and purified similarly to **2** with the following masses and volumes: 2.493 g (16.0 mmol) of bis(2-chloroethyl)methylamine, 1.102 g (47.9 mmol) of sodium metal and 5.1 ml (47.9 mmol) of butanethiol. The product was obtained as a yellow oil. Yield: 81%. ^1H NMR (400 MHz, $CDCl_3$): δ 0.90 (t, 6H, $CH_3CH_2CH_2CH_2$-S, *J* = 7.3 Hz), 1.44–1.35 (m, 4H, $CH_3CH_2CH_2CH_2$-S), 1.60–1.52 (m, 4H, $CH_3CH_2CH_2CH_2$-S), 2.28 (s, 3H, C*H*$_3$-N), 2.52 (t, 4H, $CH_3CH_2CH_2CH_2$-S, *J* = 7.3 Hz), 2.61 (br s, 8H, CH_2CH_2-N). ^{13}C APT NMR (400 MHz, $CDCl_3$): δ 13.69 ($CH_3CH_2CH_2CH_2$-S) neg, 22.00 ($CH_3CH_2CH_2CH_2$-S) pos, 29.67 (CH_2CH_2-N) pos, 31.87 ($CH_3CH_2CH_2CH_2$-S) pos, 32.11 ($CH_3CH_2CH_2CH_2$-S) pos, 42.17 (CH_3-N) neg 57.44 (CH_2CH_2-N) pos. HRMS ESI (*m*/*z*) Calcd for: $C_{13}H_{30}NS_2$ = 264.1820. Found: 264.1828. IR ν_{max} (cm^{-1}): 2956 (m), 2927 (m), 2872 (w), 2789 (w), 1458 (s), 1053 (m), 745 (m).

2.7. Bis(methylthioethyl)phenylamine (4)

Sodium methanethiolate (0.601 g, 8.58 mmol) was added to a solution of bis(2-tosylethyl)phenylamine (1.389 g, 2.84 mmol) in THF (50 ml) and the resultant mixture was left to reflux for 24 h. The reaction mixture was filtered and the solvent was removed *in vacuo* to yield a pale yellow oil. Yield: 71%. ^1H NMR (400 MHz, $CDCl_3$): δ 2.10 (s, 6H, C*H*$_3$-S), 2.62 (t, 4H, CH_2CH_2-N, *J* = 7.5 Hz), 3.48 (t, 4H, CH_2CH_2-N, *J* = 7.5 Hz), 6.59–6.65 (m, 3H, Ph-N), 7.16 (t, 2H, Ph-N, *J* = 8.0 Hz). ^{13}C APT NMR (400 MHz, $CDCl_3$): δ 15.80 (CH_3-S) neg, 31.36 (CH_2CH_2-N) pos, 51.06 (CH_2CH_2-N) pos, 111.83 (Ph-N) neg, 116.65 (Ph-N) neg, 129.43 (Ph-N) neg, 146.79 (Ph-N) pos. HRMS ESI (*m*/*z*) Calcd for: $C_{12}H_{20}NS_2$ = 242.1037. Found: 242.1031. IR ν_{max} (cm^{-1}): 3092 (w), 3034 (w), 2958 (w), 2914 (m), 1597 (s), 1501 (s), 1350 (m), 1186 (m), 745 (s), 691 (s).

2.8. Bis(ethylthioethyl)phenylamine (5)

Sodium metal (0.194 g, 8.45 mmol) and ethanethiol (0.63 ml, 8.45 mmol) were stirred together in EtOH (100 ml) under inert atmosphere for 15 min in a 250 ml Schlenk flask. This mixture was then transferred to a solution of *bis*(2-tosylethyl)phenylamine (1.378 g, 2.82 mmol) in THF (80 ml) via cannula at 0 °C and the resultant solution was refluxed for 2 h whilst monitoring by TLC. The mixture was then poured into 100 ml of double distilled water and extracted three times with 50 ml portions of DCM. The organics were combined, washed with a brine solution and dried with $MgSO_4$. The product was obtained as a pale yellow oil upon evacuation of the solvent. Yield: 73%. ^{1}H NMR (400 MHz, $CDCl_3$): δ 1.29 (t, 6H, C*H*$_3$CH$_2$-S, *J* = 7.6 Hz), 2.62 (q, 4H, CH$_3$C*H*$_2$-S), 2.73 (t, 4H, C*H*$_2$CH$_2$-N, *J* = 7.5 Hz), 3.54 (t, 4H, CH$_2$C*H*$_2$-N, *J* = 7.6 Hz), 6.71–6.65 (m, 3H, Ph-N), 7.24 (t, 2H, Ph-N, *J* = 8.1 Hz). ^{13}C APT NMR (400 MHz, $CDCl_3$): δ 15.00 (*C*H$_3$CH$_2$-S) neg, 26.27 (CH$_3$*C*H$_2$-S) pos, 28.88 (*C*H$_2$CH$_2$-N) pos, 51.51 (CH$_2$*C*H$_2$-N) pos, 111.80 (Ph-N) neg, 116.58 (Ph-N) neg, 129.54 (Ph-N) neg, 146.77 (Ph-N) pos. HRMS ESI (*m*/*z*) Calcd for: $C_{14}H_{24}NS_2$ = 270.1350. Found: 270.1345. IR ν_{max} (cm^{-1}): 3025 (w), 2962 (w), 2924 (w), 2869 (w), 1597 (s), 1502 (s), 1349 (m), 1185 (m), 744 (s), 691 (s).

2.9. Bis(cyclohexylthioethyl)phenylamine (6)

This ligand was synthesized using the same method as for **5** with the following masses and volumes: 3.085 g (6.31 mmol) of bis(2-tosylethyl)phenylamine, 0.432 g (18.92 mmol) of sodium and 2.32 ml (18.92 mmol) of cyclohexanethiol. The product was obtained as a waxy solid. Yield: 84%. ^{1}H NMR (400 MHz, $CDCl_3$): δ 1.35–1.27 (m, 12H, C$_6$H$_{12}$-S), 1.79 (m, 4H, C$_6$H$_{12}$-S), 1.99–1.93 (m, 4H, C$_6$H$_{12}$-S), 2.73 (t, 4H, C*H*$_2$CH$_2$-N, *J* = 7.5 Hz), 3.51 (t, 4H, CH$_2$C*H*$_2$-N, *J* = 7.5 Hz), 6.70–6.65 (m, 3H, Ph-N), 7.23 (t, 2H, Ph-N, *J* = 7.5 Hz). ^{13}C APT NMR (400 MHz, $CDCl_3$): δ 25.80 (C$_6$H$_{12}$-S) pos, 26.12 (C$_6$H$_{12}$-S) pos, 27.28 (*C*H$_2$CH$_2$-N) pos, 33.90 (C$_6$H$_{12}$-S) pos, 43.81(C$_6$H$_{12}$-S) neg, 51.85 (CH$_2$*C*H$_2$-N) pos, 111.83 (Ph-N) neg, 116.48 (Ph-N) neg, 129.51 (Ph-N) neg, 146.77 (Ph-N), pos. HRMS ESI (*m*/*z*) Calcd for: $C_{22}H_{36}NS_2$ = 378.2289. Found: 378.2279. IR ν_{max} (cm^{-1}): 3087 (w), 3058 (w), 3022 (w), 2923 (s), 2849 (m), 1595 (m), 1503 (s), 745 (s).

2.10. Tri-μ-chlorido-bis[bis(methylthioethyl)methylaminenickel(II)] chloride (7)

An EtOH solution (3 ml) of ligand **1** (0.190 g, 1.06 mmol) was added to a 5 ml solution of Ni(DME)Cl$_2$ (0.201 g, 1.06 mmol) in EtOH. The resultant green solution was left to stir overnight at room temperature. The solvent was then evacuated and the green residue was stirred in 5 ml of Et$_2$O to obtain a green solid which was washed several time with Et$_2$O and collected by filtration. Yield: 45%. Melting point: 253–255 °C. HRMS ESI (*m*/*z*) Calcd for: $[(C_7H_{17}NS_2)_2Ni_2Cl_3]^+$ = 578.94. Found: 578.95. IR ν_{max} (cm^{-1}): 2973 (w), 2922 (m), 2868 (m), 1463 (m), 1448 (m), 1420 (s), 1251 (m), 1018 (m), 739 (s). Anal. (%) calc. for $C_{14}H_{38}N_2S_4Cl_4Ni_2O_2$: C, 25.71; H, 5.86; N, 4.28; found: C, 25.47; H, 5.37; N, 3.96.

2.11. Tri-μ-chlorido-bis[bis(ethylthioethyl)methylaminenickel(II)] chloride (8)

Complex **8** was synthesized according to the procedure described for **7** with the following masses: 0.165 g (0.80 mmol) of **2** and 0.151 g (0.80 mmol) of Ni(DME)Cl$_2$. Yield: 74%. Melting point: 175–176 °C. HRMS ESI (*m*/*z*) Calcd for: $[(C_9H_{21}NS_2)_2Ni_2Cl_3]^+$ = 635.0000. Found: 635.0000. IR ν_{max} (cm^{-1}): 2964 (w), 2928 (m), 2872 (m), 1450 (s), 1428 (m), 1259 (m), 1040 (m), 738 (m). Anal. (%) calc. for $C_{18}H_{50}N_2S_4Cl_4Ni_2O_4$: C, 28.98; H, 6.76; N, 3.75; found: C, 28.48; H, 6.21; N, 3.31.

2.12. Tri-μ-chlorido-bis[bis(butylthioethyl)methylaminenickel(II)] chloride (9)

Complex **9** was synthesized according to the procedure described for **7** with the following masses: 0.086 g (0.39 mmol) of **3** and 0.074 g (0.39 mmol) of Ni(DME)Cl$_2$. Single crystals suitable for analysis were obtained from the crude green oil. Yield: 74%. Melting point: 89–91 °C. HRMS ESI (*m*/*z*) Calcd for: $[(C_{13}H_{29}NS_2)_2Ni_2Cl_3]^+$ = 747.1255. Found: 747.1478. IR ν_{max} (cm^{-1}): 2958 (w), 2930 (m), 2871 (m), 1463 (s), 1426 (m), 1224 (m), 1043 (m), 736 (s). Anal. (%) calc. for $C_{26}H_{68}N_2S_4Cl_4Ni_2O_5$: C, 35.64; H, 7.82; N, 3.20; found: C, 35.54; H, 7.94; N, 2.85.

2.13. Dibromido[bis(methylthioethyl)phenylamine]nickel(II) (10)

A THF solution (3 ml) of ligand **4** (0.125 g, 0.519 mmol) was added to a 3 ml solution of Ni(PPh$_3$)$_2$Br$_2$ (0.383 g, 0.515 mmol) in THF. The resultant green solution was left to stir at room temperature over a period of four days. The solvent was then evacuated and the green residue was washed with several 5 ml portions of Et$_2$O. The product was then extract with 6 ml of DCM and upon evacuation of the solvent a brown solid was obtain, identified as the product. Single crystals were obtained from a DCM solution of **10** layered with Et$_2$O. Yield: 26%. Decomposes > 200 °C. HRMS ESI (*m*/*z*) Calcd for: $[C_{12}H_{19}NS_2BrNi]^+$ = 377.9496. Found: 377.9503. IR ν_{max} (cm^{-1}): 3092 (w), 3024 (w), 2958 (w), 2914 (w), 1597 (m), 1501 (s), 1350 (m), 745 (s), 691 (s). Anal. (%) calc. for $C_{12}H_{19}NS_2NiBr_2$: C, 31.34; H, 4.16; N, 3.05; found: C, 31.38; H, 4.07; N, 2.87.

2.14. Dibromido[bis(ethylthioethyl)phenylamine]nickel(II) (11)

This complex was synthesized similarly to **10** except that DCM was used as the solvent with the following masses: 0.146 g (0.543 mmol) of **5** and 0.394 g (0.530 mmol) of Ni(PPh$_3$)$_2$Br$_2$. The product was obtained as a maroon crystalline solid. Single crystals were grown from a DCM solution of **11** layered with Et$_2$O. Yield: 30%. Melting point: 178–179 °C. HRMS ESI (*m*/*z*) Calcd for: $[C_{14}H_{23}NS_2BrNi]^+$ = 405.9809. Found: 405.9814. IR ν_{max} (cm^{-1}): 3032 (w), 2963 (m), 2924 (m), 2863 (w), 1596 (m), 1588 (m), 1491 (s), 1458 (s), 1315 (m), 779 (s), 727 (s), 707 (s), 579 (s), 496 (s). Anal. (%) calc. for $C_{14}H_{23}Br_2NNiS_2$: C, 34.46; H, 4.75; N, 2.87; found: C, 34.70; H, 4.85; N, 2.56.

2.15. Dibromido[bis(cyclohexylthioethyl)phenylamine]nickel(II) (12)

This complex was synthesized similarly to **11** with the following masses: 0.103 g (0.273 mmol) of **6** and 0.192 g (0.258 mmol) of Ni(PPh$_3$)$_2$Br$_2$. The product was obtained as a purple crystalline solid. Single crystals were grown from a DCM solution of **12** layered with Et$_2$O. Yield: 22%. Melting point: 190–191 °C. HRMS ESI (*m*/*z*) Calcd for: $[C_{22}H_{35}NS_2BrNi]^+$ = 514.0748. Found: 514.0740. IR ν_{max} (cm^{-1}): 2925 (m), 2851 (m), 1446 (s), 1265 (m), 998 (m), 745 (m), 693 (m). Anal. (%) calc. for $C_{22}H_{35}NS_2NiBr_2$: C, 44.32; H, 5.92; N, 2.35; found: C, 44.31; H, 5.87; N, 2.55.

2.16. Crystallographic analyses

Single crystals for each complex were individually selected and glued onto the tip of a glass fiber, mounted in a stream of cold nitrogen and centered in the X-ray beam using a video camera. Single-crystal X-ray diffraction data were collected on a Bruker KAPPA APEX II DUO diffractometer using graphite-monochromated Mo-

Kα radiation (χ = 0.71073 Å). Data collection was carried out at 100(2) or 173(2) K. Temperature was controlled by an Oxford Cryostream cooling system (Oxford Cryostat). Cell refinement and data reduction were performed using the program *SAINT* [49]. The data were scaled and absorption correction performed using *SADABS* [50]. The structures were solved by direct methods using *SHELXS* [50] and refined by full-matrix least-squares methods based on F^2 using *SHELXL* [50] and using the graphics interface program *X-Seed* [51,52]. All non-hydrogen atoms were refined anisotropically. All hydrogen atoms were placed in idealised positions and refined in riding models with U_{iso} assigned 1.2 or 1.5 times U_{eq} of their parent atoms and the bond distances were constrained to 0.98 or 0.99 Å. Selected crystallographic and structural refinement data are available as Electronic Supporting Information (ESI, Table S1). Crystallographic data for the structures in this article have been deposited with the Cambridge Crystallographic Data Centre, CCDC 1555285-1555288 for **9** – **12** respectively. These data can be obtained free of charge at http://www.ccdc.cam.ac.uk/conts/retrieving.html (or from the Cambridge Crystallographic Data Centre, 12 Union Road Cambridge CB2 1EZ, UK; Fax: +44-1223/336-033; E-mail: deposit@ccdc.cam.ac.uk).

2.17. Paraffin oxidation studies

The catalytic reactions were carried out in 25 ml two-neck pear shaped flasks fitted with a condenser and charged with acetonitrile as the solvent, cyclopentanone as the internal standard, *n*-octane as the paraffinic substrate and *t*-butyl hydroperoxide (TBHP) or H_2O_2 as the oxidant with the total volume of the reaction mixture equating to 5 ml. The catalyst was introduced in the form of a stock solution with the volumes varied so that the No. of moles of catalyst remained constant at 9.56 x 10^{-6} mol. The catalyst to substrate ratio was kept constant at 1:100 and the substrate to oxidant ratio was varied in order to determine the optimum amount of oxidant required for the reaction. The reactions were stirred in an oil bath maintained at 50 °C for a period of 24 h after which a sample was removed, treated with an excess amount of PPh_3 (until the sample was saturated) and filtered through a Celite plug. Thereafter, a 0.5 μl aliquot was injected into the GC for analysis and quantification of the products. The products were analysed using a PerkinElmer Auto System gas chromatograph equipped with a flame ionisation detector (FID) which was set at 260 °C. A 50 m × 0.20 mm × 0.5 μm Pona column was employed to efficiently separate the products with the injector temperature set at 240 °C. Yield was calculated based on the total moles of products formed divided by the initial moles of substrate added into the reaction mixture and was expressed as a percentage, while the selectivity was expressed as the mole fraction of each product expressed as a percentage. All catalytic reactions were performed in duplicate. Each reported data was replicated within acceptable variance.

3. Results and discussion

3.1. Synthesis and characterization of ligands

This study reports on the synthesis and characterization of six pincer-type SNS ligands, (the majority of which are new) and the coordination chemistry of their Ni complexes. The SNS ligands prepared contained a flexible, straight chained amine backbone functionalised with a methyl or phenyl group as well as ethylene linkers to the S-donor atoms. The substituents bonded to the S-donor atoms were varied to investigate steric and electronic effects on the complexes. The synthetic route followed for the preparation of the ligands and complexes was developed and optimised to obtain the best yield and purity of the compounds.

All the ligands (Scheme 1) were synthesized by the reaction of bis(2-chloroethyl)methylamine or bis(2-tosylethyl)phenylamine with the respective thiol, which was activated by stirring with sodium metal in ethanol, to form the products as oils (with the exception of **6**) in 71–84% yields. The ligands were purified on a silica gel column and characterised by NMR, IR and HRMS.

NMR experiments (^{1}H and ^{13}C APT) were employed to elucidate the structures of the ligands prepared, since these are reliable and efficient techniques that provide important characterisation data. Spectra obtained for each ligand showed clean signals which integrated to the expected number of protons with no signs of impurities present. An analysis of the results revealed that the methyl group bonded to the central *N*-donor atom on the ligand backbone appeared as a singlet in the region of 2.27–2.28 ppm for **1**–**3**. The two symmetric ethylene linker groups gave rise to a multiplet or a broad signal between 2.59 and 2.61 ppm which integrated to the expected eight protons. In contrast, two triplets of four protons each were observed for the ethylene spacers of the phenyl substituted ligands **4**–**6**.

An HSQC NMR experiment (see Supplementary Information) was undertaken to highlight the correlation between the broad sig-

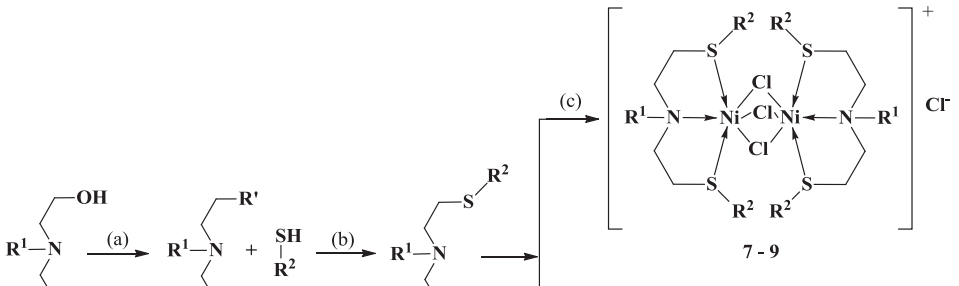

1: R^1 = Me, R^2 = Me **4**: R^1 = Ph, R^2 = Me
2: R^1 = Me, R^2 = Et **5**: R1 = Ph, R2 = Et
3: R^1 = Me, R^2 = Bu **6**: R^1 = Ph, R^2 = Cy

7: R^1 = Me, R^2 = Me; **8**: R^1 = Me, R^2 = Et; **9**: R^1 = Me, R^2 = Bu
10: R^1 = Ph, R^2 = Me; **11**: R^1 = Ph, R^2 = Et; **12**: R^1 = Ph, R^2 = Cy

Scheme 1. Synthetic route to the synthesis of ligands **1**–**6** and Ni complexes **7**–**12**. (a): $SOCl_2$ or TsCl, (b): Na/C_2H_5OH mixture, (c): Ni(DME)Cl_2 and (d): Ni$(PPh_3)_2Br_2$.

nal of **2** and the related carbon atoms. It shows that all the associated eight protons are equivalent to each other and are in the same environment, hence the overlapping signals. For the second series of ligands functionalised by the phenyl *N*-backbone (**4**–**6**), the aromatic protons were all observed as expected further downfield in the region of 6.61–7.24 ppm. The data obtained from IR and HRMS analyses are all as expected for each of the prepared ligands.

3.2. Synthesis and characterisation of complexes

The reaction of a slight molar excess of the respective SNS ligands (L) {[L = $(RSCH_2CH_2)_2NMe$: where R = Me (**1**), Et (**2**), Bu (**3**)] or [L = $(RSCH_2CH_2)_2NPh$: where R = Me (**4**), Et (**5**), Cy (**6**)]} with the metal salts $(Ni(DME)Cl_2$ or $Ni(PPh_3)_2Br_2)$ resulted in the formation of new cationic dimeric $[LNi(\mu\text{-}Cl)_3NiL]^+$ (**7**–**9**) and mononuclear ($LNiBr_2$) **10**–**12** complexes (Scheme 1). It is important to note that the relatively bulkier and rigid groups around the Ni(II) centres in complexes **10**–**12** are responsible for the monomeric nature of these complexes in comparison to the dimeric **7**–**9**. Complexes **10**–**12** bear planar phenyl substituents on the *N*-donor atoms in comparison to the methyl *N*-substituents of **7**–**9** and in addition, the former contain larger bromido ligands in comparison to the chlorido-bearing **7**–**9**. These reasons combine to explain the structural differences between the two sets of NiSNS pincer complexes. At the start of the reaction, an immediate colour change was observed to indicate successful Ni complexation to the ligand. Due to unresolved NMR signals, which we attributed to the paramagnetic nature of nickel in the +2 state, we used other characterisation techniques. These included IR, MS, elemental analysis and single crystal XRD for selected complexes, to analyse and unambiguously confirm the structural composition and purity of all the new Ni complexes.

The prepared NiSNS complexes are hygroscopic and absorbed moisture upon exposure to air. This was evident from the broad band observed in the O–H stretching region of their IR spectra. Nevertheless, upon complexation, significant shifts in the frequencies of bands associated with the SNS ligands were noted and interpreted as indicators of successful coordination of the isolated SNS ligands to the Ni(II) centres. From the selected data listed in Table 1 for complexes **7**–**9**, it is clear that enhanced dπ-pπ overlap between the nickel metal centre and the *N*-donor atom of the SNS moiety occurred upon coordination with the consequence that the ligand C–N bond weakened while the alkyl C–H stretch strengthened, as shown by the IR results (see ESI).

ESI-MS data for all the metal complexes (**7**–**12**) displayed the $[NiSNSX]^+$ ion (where X = Cl or Br) as the predominant species and the specific isotopic patterns found were consistent and in line with what is expected for halogenated complexes. Furthermore, we observed for complexes **7**–**9**, a mass corresponding to a dimer linked by three chlorides. This suggested that these complexes possibly dimerise via three bridging chlorido groups. The observation was later confirmed by X-ray crystallographic data of **9**. However, this pattern was not observed for complexes **10**–**12** bearing the phenyl *N*-substituent. The CHN analyses obtained for complexes **7**–**9** revealed the presence of varying amounts of water in the sample which was expected due to the hygroscopic nature of these complexes. The data acquired for complexes **10**–**12** were within the acceptable range which is indicative of their high purity.

Table 1
Selected IR data for ligands (**1**–**3**) and the corresponding nickel complexes (**7**–**9**).

Compound	IR ν_{max}/cm^{-1}		
	C–H stretch[a]	C–H bend[a]	C–N stretch[b]
1	2915	1456	1056
7	2922	1464	1048
2	2925	1453	1050
8	2930	1449	1040
3	2927	1458	1053
9	2930	1464	1043

[a] Strong.
[b] Medium.

3.3. Single crystal X-ray structural analysis of complexes

Green single crystals were grown for complex **9** from a crude green oil and for complexes **10**–**12** from DCM solutions layered with diethyl ether to yield dark brown to purple crystals. Complex **9** was isolated as a bimetallic dimer with octahedral geometry around each Ni(II) centre (Fig. 1), while complexes **10**–**12** (Figs. 2 and 3 respectively) crystallised as monomeric five coordinate complexes that are characterised by trigonal bipyramidal geometry around the metal.

Complex **9** crystallised in the triclinic $P\bar{1}$ space group as dimeric species containing distorted octahedrally bonded Ni(II) centres (Fig. 1) bridged via three chloride substituents. Related NiSNS complexes with halogen bridging have been reported in the literature [53,54]. The tridentate SNS ligand chelates in a facial binding mode to the metal centre such that the S-donor atoms, Cl(1) and Cl(3) lie in the same equatorial plane, while the *N*-donor atoms and Cl(2) occupy axial positions of the octahedron. The coordination environment around Ni(2) is identical to that of Ni(1).

The two octahedral metal centres are separated by a Ni···Ni distance of 3.018 Å which is shorter than the sum of the van der Waals radii for two nickel atoms (3.260 Å). Therefore, it can be regarded as a relatively strong interaction, specifically in comparison to the previously reported CoSNS complex [39] which displayed a Co···Co distance of 3.684 Å and a related tetradentate Ni complex containing an asymmetric pyrazolate ligand with a Ni···Ni distance of 3.823 Å [43]. Although it is quite rare to find Ni complexes that are bridged via three chlorides, there are a few reports on related complexes [55–57]. One such is reported by Wikstrom et al., which contains a tridentate NNN ligand [57]. A Ni···Ni distance of 3.086 Å was calculated for this complex, which is still slightly longer than what is observed for **9**. The crystal packing between molecules of **9** displayed a head-to-head, tail-to-tail arrangement of the crystal units with the head being the methylene group and the tail referring to the butyl chains.

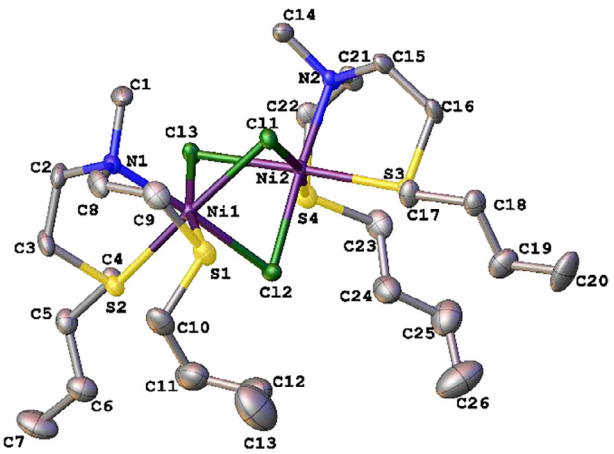

Fig. 1. Molecular structure of **9** with hydrogen atoms omitted for clarity. Thermal ellipsoids are drawn at the 50% probability level. Selected bond lengths (Å) and angles (°): N(1)–Ni(1), 2.135(2); S(1)–Ni(1), 2.3857(8); S(2)–Ni(1), 2.4168(7); Cl(1)–Ni(1), 2.4303(7); Cl(2)–Ni(1), 2.4159(7); Cl(3)–Ni(1), 2.4562(7); S(1)–Ni(1)–S(2), 97.95(3); N(1)–Ni(1)–S(1), 87.42(7); N(1)–Ni(1)–S(2), 85.49(6); N(1)–Ni(1)–Cl(1), 97.11(6); N(1)–Ni(1)–Cl(2), 176.50(6); N(1)–Ni(1)–Cl(3), 94.06(7).

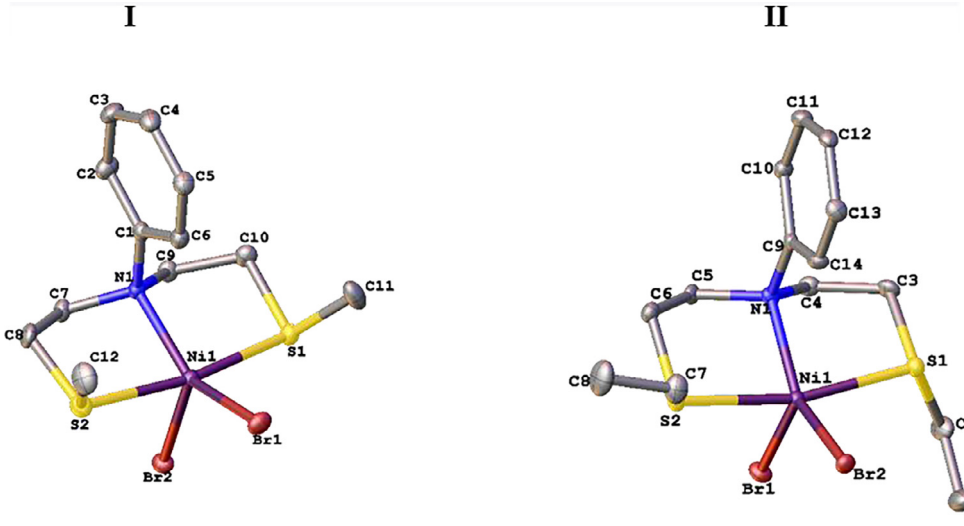

Fig. 2. Molecular structures of **10** (I) and **11** (II) with hydrogen atoms omitted for clarity and thermal ellipsoids shown at the 50% probability level. Selected bond lengths (Å) and angles (°) for **10**: N(1)–Ni(1), 2.106(2); S(1)–Ni(1), 2.4319(8); S(2)–Ni(1), 2.3981(8); Cl(1)–Ni(1), 2.4481(4); Cl(2)–Ni(1), 2.4147(4); S(1)–Ni(1)–S(2), 170.13(3); N(1)–Ni(1)–S(1), 85.07(7); N(1)–Ni(1)–S(2), 85.06(7); N(1)–Ni(1)–Cl(1), 100.30(6); N(1)–Ni(1)–Cl(2), 143.78(6). For **11**: N(1)–Ni(1), 2.107(2); S(1)–Ni(1), 2.4329(8); S(2)–Ni(1), 2.4310(7); Cl(1)–Ni(1), 2.4313(4); Cl(2)–Ni(1), 2.4221(4); S(1)–Ni(1)–S(2), 166.49(3); N(1)–Ni(1)–S(1), 83.27(7); N(1)–Ni(1)–S(2), 84.87(7); N(1)–Ni(1)–Cl(1), 101.02(6); N(1)–Ni(1)–Cl(2), 143.59(6).

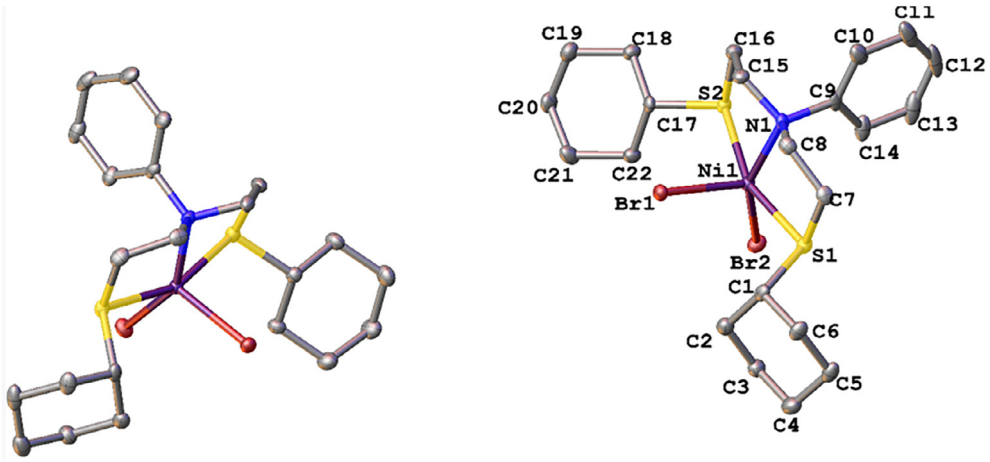

Fig. 3. Molecular structure of **12** showing two crystallographically independent molecules in the asymmetric unit cell with hydrogen atoms omitted for clarity and thermal ellipsoids shown at the 50% probability level. Selected bond lengths (Å) and angles (°): N(1)–Ni(1), 2.114(2); S(1)–Ni(1), 2.4283(9); S(2)–Ni(1), 2.4291(10); Cl(1)–Ni(1), 2.4461(5); Cl(2)–Ni(1), 2.4293(5); S(1)–Ni(1)–S(2), 158.93(3); N(1)–Ni(1)–S(1), 84.09(8); N(1)–Ni(1)–S(2), 82.97(8); N(1)–Ni(1)–Cl(1), 97.44(7); N(1)–Ni(1)–Cl(2), 148.72(8).

Complexes **10**–**12** all crystallised in the $P2_1$ space group of the monoclinic crystal system. Only **12** crystallised with two identical but independent molecules in the asymmetric unit cell as shown in Fig. 3. All three complexes exhibit a five coordinate, distorted trigonal bipyramidal geometry around the metal with the S-donor atoms occupying axial positions and the equatorial sites taken up by the *N*-donor and the two bromide substituents.

The phenyl ring, N(1), Ni(1), Br(1) and Br(2) reside in the same plane for complexes **10** and **11** (Fig. 2) with this also serving as a plane of symmetry in **10**. However, for **12**, the phenyl ring deviates from the [N(1), Ni(1), Br(1), Br(2)] plane by 0.026–0.500 Å. The general trend observed is that as the flexibility of the substituents on the S-donor atoms increased, the degree of asymmetry of the entire complex also increased. Furthermore, the 'bite angle' defined by the S(1)–Ni(1)–S(2) chelation gradually became more acute as the substituents (R) on the S-donor atoms increased in steric complexity [methyl = 170.13(3), ethyl = 166.49(3) and cyclohexyl = 158.93(3)°]. This can be attributed to an increased steric crowding around the metal centre resulting in a decreased 'bite angle'.

An observation of the crystal packing of **10**–**12** revealed a similar ordered arrangement of alternating units forming parallel sheets in a head-to-tail configuration, where the phenyl and bromide groups define the head and tail of the molecule respectively. Intriguingly, the cyclohexyl groups present in **12** do not hinder the packing efficiency of the molecule in the crystal lattice, which resulted in a more closely packed arrangement as compared to **10** and **11** (See the ESI for packing Figures).

3.4. Application of the NiSNS complexes in n-octane oxidation

The prepared nickel complexes were applied as catalysts in the oxidation of *n*-octane with both H_2O_2 and *tert*-butyl hydroperoxide (TBHP) as the source of oxygen in acetonitrile medium. Tests using H_2O_2 as the oxidant gave yields equivalent to that of the blank

reaction (absence of catalyst) over 24 h (1–2%), which indicate that the catalysts were inactive for C—H functionalisation with this particular oxidant. A colour change from green to colourless was also observed upon the addition of H_2O_2, which is indicative of catalyst decomposition. Therefore, TBHP was investigated further, since it is a milder oxidant in comparison to H_2O_2.

Preliminary studies established the optimum conditions for the oxidation reaction as 50 °C, at a catalyst to octane to TBHP ratio of 1:100:1200 and a reaction time of 48 h (data was also recorded at 24 h). The cost and efficiency of utilising the oxidant is critical in the successful adoption of any oxidation catalyst system, hence the octane to TBHP ratio was thoroughly investigated (1:3, 1:6, 1:9, 1:12, 1:15 and 1:18), however, the best balance between yield and product selectivity was observed at 1:12 substrate to oxidant ratio. A blank reaction gave a yield of 2% in 48 h, while reactions with the simple salts ($NiCl_2$ and $NiBr_2$) gave yields of 3 and 5% respectively. Catalytic data highlighting yields to total oxidation products for all the complexes is presented in Fig. 4.

The yields were calculated after treatment of the reaction aliquot with PPh_3, in order to reduce any octyl hydroperoxides present in the sample. This is a standard and largely accepted procedure for paraffin oxidation reactions first developed and reported by the Shul'pin group [58].

For catalysts **7**–**9**, bearing the sterically smaller *N*-substituent, it is clear that the yields are substantially higher than that over the metal precursor ($NiCl_2$). This suggests that the ligands influenced the enhanced activities of the catalysts. Furthermore, a slight increase in yield was observed on extending the time of reaction from 24 to 48 h, with **7** giving the highest yield of 9% at 48 h. The ligand of this catalyst contains the smallest R-substituent bonded to the S-donor atoms ($-CH_3$) which resulted in the least sterically hindered metal centre. The metal centre is the active site to which the substrate binds, hence in theory, a more sterically available metal centre should render higher activity than a congested one that offers constrained access to the substrate *n*-octane. This indicates the role of the ligand in determining the availability of binding sites for the substrate, which ultimately determines catalyst efficiency. The yield then drops to 7% for **8**, presumably because of an increase in the steric crowding around the metal centre caused by the S-donor ethyl substituent. However, the slight increase to 8% for catalyst **9** can be attributed to an electronic effect caused by the electron donating long chain butyl groups.

The catalytic activities of the more rigid phenyl *N*-substituted catalysts showed a different trend to those of the methyl *N*-substituted series. Catalyst **10**, containing the methyl substituents on the S-donor atoms was the least active giving a yield only marginally higher than that of the metal precursor at 48 h. However, **11**, substituted with ethyl groups on the S-donor atoms, gave a significantly higher yield of 10% at 48 h. This suggests that electronic effects and increased hydrophobicity dominate the catalytic activity, since the ethyl groups are better electron donors and more hydrophobic than the methyl substituents. Although catalyst **12** is electronically the richest in the series due to the cyclohexyl S-substituents, in comparison to **11**, a lower yield was recorded indicating that both electronic and steric effects contribute to the catalytic activity. The cyclohexyl rings contributed to a degree of steric crowding around the active site which slightly decreased its activity.

Product selectivity is an important aspect in determining the efficiency of a catalytic system. Obtaining a single product would be ideal but also unrealistic especially in the oxidation of *n*-octane. Considering the product distribution pattern obtained for both catalyst series, a mixture of octanols and octanones oxygenated at carbon positions 2, 3 and 4 (C-2, C-3 and C-4) of the octane C-8 backbone was observed. No terminal carbon (C-1) activation was recorded for any of the systems in this study. The combined alcohol and ketone selectivities for **7** are presented in Fig. 5, from which the following points are observed:

- Octanones represent the majority product class at both 24 and 48 h reaction periods.
- Accumulation of the ketones seems to be a secondary reaction of alcohol over-oxidation. This is clear from the increased ketone selectivity at 48 h which is matched by decreased alcohol selectivity.

It is also important to note that a similar trend is observed for the rest of the catalysts, indicating that they all followed a similar reaction pathway.

The product distribution pattern, which displays the individual product selectivities as well as the regioselectivity parameters at each carbon, i.e. C(2):C(3):C(4) is presented in Table 2. Amongst the methyl *N*-substituted catalysts, **7** and **9** showed higher selectivity to the ketone products with low alcohol/ketone (*A*/*K*) ratios of 0.28 and 0.30 respectively. Overall, catalyst **10** is the most selective to the alcohols with the highest *A*/*K* ratio of 2.13, presumably because of its comparatively lower activity. Hence, its ability to further oxidize the initial alcohol products to ketones was also low, meaning that at the end of the reaction period, more of the alcohol products remain. A low *A*/*K* ratio of 0.35 was observed for **11** and this can be attributed to the higher activity it displayed, which further emphasizes our belief that over-oxidation, driven by a very active catalyst, is responsible for the prevalence of ketone products in this systems.

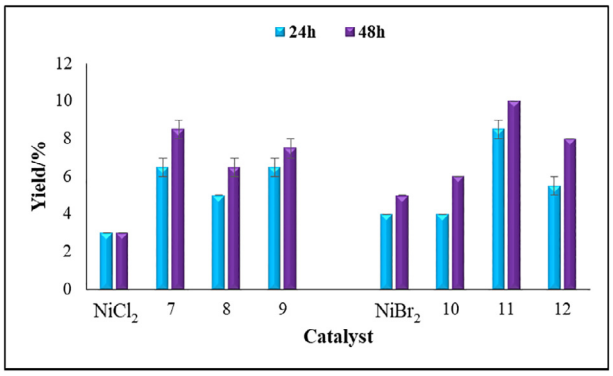

Fig. 4. Yields obtained for the catalysts bearing the methyl *N*-substituent (**7**–**9**) and phenyl *N*-substituent (**10**–**12**). Conditions: octane:TBHP = 1:12, Temp = 50 °C, Time = 24 and 48 h.

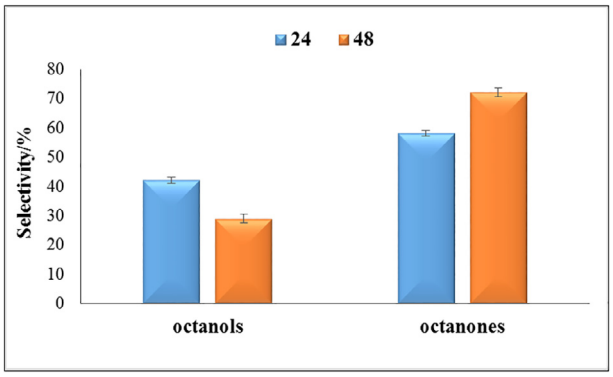

Fig. 5. Selectivities to combined alcohol and ketone products for catalyst **7**. Conditions: Octane:TBHP = 1:12, Temp = 50 °C, Time = 24 and 48 h.

Table 2
Product selectivity and regioselectivity parameters in the oxidation of *n*-octane.[a]

	Product selectivity (%)							*A*/*K*[c]
Catalyst	2-ol	3-ol	4-ol	2-one	3-one	4-one	C(2):C(3):C(4)[b]	
7	10	6	6	28	24	26	1.3:1:1.1	0.28
8	26	12	12	18	15	17	1.5:1:1	1.00
9	11	6	6	29	22	26	1.5:1:1.2	0.30
10	34	17	17	10	10	12	1.7:1:1.1	2.13
11	13	7	6	28	21	25	1.4:1:1.1	0.35
12	18	9	9	23	18	23	1.6:1:1.2	0.56
$NiCl_2$	31	14	13	14	13	15	1.7:1:1	1.38
$NiBr_2$	23	10	10	20	17	20	1.6:1:1.1	0.75

[a] Reaction conditions: catalyst (9.56×10^{-6} mol, 1.91×10^{-3} M), *n*-octane (9.56×10^{-4} mol, 0.155 ml), TBHP (70% in H_2O, 0.0164 mol), 50 °C, 48 h, MeCN added as a solvent to give a total reaction volume of 5 ml.
[b] Total regioselectivity parameter takes into consideration both alcohol and ketone products at each carbon position and these values are normalized, i.e. taking into account the number of hydrogen atoms, 3 for the terminal carbon (CH_3) and 2 for each of the unique internal carbon (CH_2) positions.
[c] *A*/*K* ratio gives the relative selectivity irrespective of carbon position of all alcohol/all ketone products, i.e. total moles of octanols divided by total moles of octanones.

In line with literature reports, the total regioselectivity parameter indicated that the internal C(2) hydrogens of the *n*-octane chain were the most reactive [59–61]. Results obtained in this study are comparable to those reported by Pombeiro and co-workers using a Mn(salen) catalyst with TBHP [59]. They had also observed no C(1) activation and reported similar regioselectivity numbers for the oxidation of *n*-octane.

In order to gain an insight into the mechanistic pathway, a reaction was conducted under our standard conditions with catalyst **11** in the presence of a radical inhibitor, TEMPO. No products were detected in this reaction, thus indicating that the mechanism follows a radical pathway as described in numerous literature reports [58,59,62,63].

4. Conclusion

In this work, six pincer-type SNS ligands were prepared, characterised and coordinated to Ni(II) to yield six new complexes which have also been fully characterised. The Ni complex **9**, with butyl substituents on the S-donor atoms, crystallised as an unusual three chlorido-bridged homo bimetallic dimer. The NiSNS complexes, characterised by a phenyl functionality on the *N*-donor atom, crystallised as monomeric species with the SNS ligand coordinated in a tridentate fashion around each trigonal bipyramidal Ni(II) centre.

All the complexes were utilised as catalysts in the oxidation of *n*-octane with TBHP as the oxidant. No products of terminal or C(1) carbon activation were observed for any of the catalysts studied. Furthermore, no cracking of the octane chain was detected and only C-8 products were observed. Overall, catalyst **11** was the most active with a total product yield of 10%, whilst **10** was the least active and most selective to alcohol products. The highest selectivity to the ketone products was seen for **7**. Analysis of the regioselectivity revealed that the C(2) position on the *n*-octane chain was the most prominent position of attack for all the catalytic systems studied in this work.

Acknowledgements

We are very grateful to the University of KwaZulu-Natal, c∗ change and the NRF for financial support. We thank Dr Hong Su, Dr Michael Nivendran Pillay and Mr Sizwe Zamisa for X-ray crystallographic data collection and refinement.

Appendix A. Supplementary data

Supplementary data associated with this article can be found, in the online version, at https://doi.org/10.1016/j.ica.2018.04.033.

References

[1] C.J. Moulton, B.L. Shaw, J. Chem. Soc. Dalton Trans. (1976) 1020–1024.
[2] J.T. Singleton, Tetrahedron 59 (2003) 1837–1857.
[3] D. Morales-Morales, Revista de la Sociedad Química de Mexico 48 (2004) 338–346.
[4] S.B. Harkins, J.C. Peters, Organometallics 21 (2002) 1753–1755.
[5] C. Gunanathan, D. Milstein, Chem. Rev. 114 (2014) 12024–12087.
[6] N. Selander, K.I.n.J. Szabó, Chem. Rev. 111 (2010) 2048–2076.
[7] D.M. Spasyuk, S.I. Gorelsky, A. van der Est, D. Zargarian, Inorg. Chem. 50 (2011) 2661–2674.
[8] R.A. Baber, R.B. Bedford, M. Betham, M.E. Blake, S.J. Coles, M.F. Haddow, M.B. Hursthouse, A.G. Orpen, L.T. Pilarski, P.G. Pringle, R.L. Wingad, Chem. Commun. (2006) 3880–3882.
[9] D. Gelman, S. Musa, ACS Catal. 2 (2012) 2456–2466.
[10] Z. Tang, E. Otten, J.N.H. Reek, J.I. van der Vlugt, B. de Bruin, Chem. Eur. J. 21 (2015). 12529 12529.
[11] M.E. Pascualini, N.V. Di Russo, P.A. Quintero, A.E. Thuijs, D. Pinkowicz, K.A. Abboud, K.R. Dunbar, G. Christou, M.W. Meisel, A.S. Veige, Inorg. Chem. 53 (2014) 13078–13088.
[12] B.-S. Zhang, W. Wang, D.-D. Shao, X.-Q. Hao, J.-F. Gong, M.-P. Song, Organometallics 29 (2010) 2579–2587.
[13] M.-J. Yang, Y.-J. Liu, J.-F. Gong, M.-P. Song, Organometallics 30 (2011) 3793–3803.
[14] D. Morales-Morales, Mini-Rev. Org. Chem. 5 (2008) 141.
[15] J.M. Serrano-Becerra, D. Morales-Morales, Curr. Org. Synth. 6 (2009) 169.
[16] G. Van Koten, D. Milstein, Organometallic Pincer Chemistry, Springer, Berlin, Heidelberg, 2013.
[17] K.J. Szabó, O.F. Wendt, Pincer and Pincer-type Complexes: Applications in Organic Synthesis and Catalysis, Wiley-VCH, 2014.
[18] C. Gunanathan, D. Milstein, Acc. Chem. Res. 44 (2011) 588.
[19] M. Asay, D. Morales-Morales, Dalton Trans. 44 (2015) 17432–17447.
[20] H. Valdés, L. González-Sebastián, D. Morales-Morales, J. Organomet. Chem. 845 (2017) 229–257.
[21] D. Morales-Morales, C.M. Jensen, The Chemistry of Pincer Compounds, Elsevier, Amsterdam, 2007.
[22] J.I. van der Vlugt, J.N.H. Reek, Angew. Chem. Int. Ed. 48 (2009) 8832–8846.
[23] D. Milstein, Top. Catal. 53 (2010) 915–923.
[24] W.-G. Jia, D.-D. Li, H. Zhang, Y.-C. Dai, E.-H. Sheng, J. Coord. Chem. 68 (2014) 220–228.
[25] Y. Klerman, E. Ben-Ari, Y. Diskin-Posner, G. Leitus, L.J.W. Shimon, Y. Ben-David, D. Milstein, Dalton Trans. (2008) 3226–3234.
[26] D.S. McGuinness, D.B. Brown, R.P. Tooze, F.M. Hess, J.T. Dixon, A.M.Z. Slawin, Organometallics 25 (2006) 3605–3610.
[27] D.S. McGuinness, P. Wasserscheid, D.H. Morgan, J.T. Dixon, Organometallics 24 (2005) 552–556.
[28] D.S. McGuinness, P. Wasserscheid, W. Keim, D. Morgan, J.T. Dixon, A. Bollmann, H. Maumela, F. Hess, U. Englert, J. Am. Chem. Soc. 125 (2003) 5272–5273.
[29] K. Albahily, Y. Shaikh, Z. Ahmed, I. Korobkov, S. Gambarotta, R. Duchateau, Organometallics 30 (2011) 4159–4164.
[30] C.N. Temple, S. Gambarotta, I. Korobkov, R. Duchateau, Organometallics 26 (2007) 4598–4603.
[31] C. Temple, A. Jabri, P. Crewdson, S. Gambarotta, I. Korobkov, R. Duchateau, Angew. Chem. 118 (2006) 7208–7211.
[32] A. Jabri, C. Temple, P. Crewdson, S. Gambarotta, I. Korobkov, R. Duchateau, J. Am. Chem. Soc. 128 (2006) 9238–9247.
[33] S.-Q. Bai, T.S.A. Hor, Chem. Commun. (2008) 3172–3174.
[34] M.J. Page, J. Wagler, B.A. Messerle, Organometallics 29 (2010) 3790–3798.
[35] S.G. Mastrostamatis, M.S. Papadopoulos, I.C. Pirmettis, E. Paschali, A.D. Varvarigou, C.I. Stassinopoulou, C.P. Raptopoulou, A. Terzis, E. Chiotellis, J. Med. Chem. 37 (1994) 3212–3218.

[36] M.S. Papadopoulos, I.C. Pirmettis, M. Pelecanou, C.P. Raptopoulou, A. Terzis, C.I. Stassinopoulou, E. Chiotellis, Inorg. Chem. 35 (1996) 7377–7383.
[37] X. Chen, F.J. Femia, J.W. Babich, J. Zubieta, Inorg. Chim. Acta 307 (2000) 88–96.
[38] B.A. Nock, T. Maina, D. Yannoukakos, I.C. Pirmettis, M.S. Papadopoulos, E. Chiotellis, J. Med. Chem. 42 (1999) 1066–1075.
[39] L. Soobramoney, M.D. Bala, H.B. Friedrich, Dalton Trans. 43 (2014) 15968–15978.
[40] F. Teixidor, L. Escriche, J. Casabo, E. Molins, C. Miravitlles, Inorg. Chem. 25 (1986) 4060–4062.
[41] L. Canovese, G. Chessa, G. Marangoni, B. Pitteri, P. Uguagliati, F. Visentin, Inorg. Chim. Acta 186 (1991) 79–86.
[42] F. Teixidor, G. Sanchez-Castello, N. Lucena, L. Escriche, R. Kivekas, M. Sundberg, J. Casabo, Inorg. Chem. 30 (1991) 4931–4935.
[43] M. Konrad, F. Meyer, K. Heinze, L. Zsolnai, J. Chem. Soc. Dalton Trans. (1998) 199–206.
[44] D. Spasyuk, S. Smith, D.G. Gusev, Angew. Chem. Int. Ed. 52 (2013) 2538–2542.
[45] B.T. Golding, M.J. Kebbell, I.M. Lockhart, J. Chem. Soc. Perkin Trans. 2 (1987) 705–713.
[46] C.S. Park, J.Y. Lee, E.-J. Kang, J.-E. Lee, S.S. Lee, Tetrahedron Lett. 50 (2009) 671–675.
[47] B.S. Furniss, A.J. Hannaford, P.W.G. Smith, A.R. Tatchell, Vogel's Textbook of Practical Organic Chemistry, 5th edn., John Wiley & Sons Inc, New York, 1989.
[48] S.Y. Tyree, Inorganic Syntheses, John Wiley & Sons Inc, New York 4 (1953) 104.
[49] SAINT Version 7.60a, Bruker AXS Inc., Madison, WI, USA, 2006.
[50] G.M. Sheldrick, SHELXS-97, SHELXL-2014 and SADABS version 2.05, University of Göttingen, Germany, 1997.
[51] L.J. Barbour, Supramol. Chem. 1 (2001) 189–191.
[52] J.L. Atwood, L.J. Barbour, Cryst. Growth Des. 3 (2003) 3–8.
[53] M. Basauri-Molina, S. Hernández-Ortega, D. Morales-Morales, Eur. J. Inorg. Chem. 2014 (2014) 4619–4625.
[54] V.E. Márquez, J.R. Anacona, R.J. Hurtado, G. Dıaz de Delgado, E.M. Roque, Polyhedron 18 (1999) 1903–1908.
[55] A.J. Blake, M.A. Halcrow, M. Schroder, Acta Crystallographica Section C 48 (1992) 1844–1846.
[56] M.V. Baker, D.H. Brown, B.W. Skelton, A.H. White, Aust. J. Chem. 55 (2002) 655–660.
[57] J.P. Wikstrom, A.S. Filatov, R.J. Staples, C.R. Guifarro, E.V. Rybak-Akimova, Inorg. Chim. Acta 363 (2010) 884–890.
[58] G.B. Shul'pin, Mini-Rev. Org. Chem. 6 (2009) 95–104.
[59] T.C.O. Mac Leod, M.V. Kirillova, A.J.L. Pombeiro, M.A. Schiavon, M.D. Assis, Appl. Catal. A 372 (2010) 191–198.
[60] M.V. Kirillova, A.M. Kirillov, D. Mandelli, W.A. Carvalho, A.J.L. Pombeiro, G.B. Shulpin, J. Catal. 272 (2010) 9–17.
[61] D. Naicker, H.B. Friedrich, B. Omondi, RSC Adv. 5 (2015) 63123–63129.
[62] S. Förster, A. Rieker, K. Maruyama, K. Murata, A. Nishinaga, J. Organic Chem. 61 (1996) 3320–3326.
[63] A.A. Fokin, P.R. Schreiner, Chem. Rev. 102 (2002) 1551–1594.